Iron Loss Characterization in Laminated Cores at Room and Liquid Nitrogen Temperature

Iron Loss Characterization in Laminated Cores at Room and Liquid Nitrogen Temperature

Marco Biasion, *Student Member, IEEE*
Politecnico di Torino
Dipartimento Energia
Torino, Italy
marco.biasion@polito.it

Inês S. P. Peixoto, *Student Member, IEEE*
Politecnico di Torino
Dipartimento Energia
Torino, Italy
ines.peixoto@polito.it

João F. P. Fernandes, *Member, IEEE*
IDMEC, Instituto Superior Técnico
University of Lisbon
Lisbon, Portugal
joao.f.p.fernandes@tecnico.ulisboa.pt

Silvio Vaschetto, *Senior Member, IEEE*
Politecnico di Torino
Dipartimento Energia
Torino, Italy
silvio.vaschetto@polito.it

Gerd Bramerdorfer, *Senior Member, IEEE*
Institute of Electrical Drives and Power Electronics, Johannes Kepler University Linz
Linz, Austria
gerd.bramerdorfer@jku.at

Andrea Cavagnino, *Fellow, IEEE*
Politecnico di Torino
Dipartimento Energia
Torino, Italy
andrea.cavagnino@polito.it

***Abstract*— This paper presents the characterization of the magnetic properties of laminated cores for electrical machines at ambient and cryogenic temperature. Silicon-iron stator cores of different steel grades are characterized experimentally at room temperature and when immersed in a liquid nitrogen atmosphere. The magnetic characterizations involve the measurement of the normal magnetization curve, and the core losses in a wide range of frequencies and magnetic flux densities. The separation of the losses into their physical components is carried out with an energy-based approach aiming at a thorough analysis of each loss contribution. The results show that the cryogenic temperature does not significantly impact the magnetization characteristic of the material, regardless the tested steel grade. The core losses generally increase at cryogenic temperature. The separation of the losses into components shows that the hysteresis contribution is not much affected by the cryogenic temperature; the global dynamic losses increase at a rate that depends on the steel grade instead, at least in the examined frequency and flux density ranges.**

Keywords*— *Electrical steel sheets, silicon-iron sheets, magnetic characterization, core loss measurement, core loss modeling, core loss separation, cryogenics, liquid nitrogen.

I. Introduction

Cryogenic electrical machines have received much attention in recent years due to their attractive characteristics in terms of high torque density and improved efficiency. More specifically, there have been increasing efforts in developing cryogenic electrical machines featuring conventional and superconducting windings in different combinations [1], [2]. The active parts of cryogenic motors and generators can be effectively cooled by submersion into a cryogenic bath, a technology that sometimes is referred in the literature as '*wet*' cryogenics. At present, commercial cryogenic-cooled electrical machines have found their most relevant application in industrial pumps for liquefied natural gas, operating at ~110 K (−161 °C). Such machines are manufactured with conventional materials for the active parts, and their performance are usually assessed in a liquid nitrogen (LN_2) atmosphere at 77 K (−196 °C) for safety reasons.

The optimal design of cryogenic-cooled machines requires a detailed segregation of the loss phenomena in the device. A previous experimental study carried out by the authors involved the analysis of a fractional kilowatt induction machine operated in LN_2 [2]. It was shown that the core losses may take a relevant part of the total losses. Hence, the magnetic characterization of soft magnetic materials at cryogenic temperature plays a crucial role in both the analysis and the design of cryogenic-cooled electrical machines.

Various studies have been focusing their attention on the characterization of laminated steels at cryogenic temperature, investigating both the magnetization characteristics and the power losses. The characterizations reported in [3]–[6] were carried out on various materials and steel grades in the form of ring samples, under alternating flux density excitation. A similar investigation was presented in [7], but using a miniature single-sheet tester. The magnetic properties of a selected steel grade at liquid nitrogen temperature were studied in [8], under both alternating and rotational flux density excitation. The rotating flux density was achieved using the assembled stator core of a single-phase induction machine.

The manufacturing of the cores of electrical machines may negatively impact the magnetic properties of the laminations, resulting in a degradation of the quality of the steel. It turns out that the magnetic properties of the laminations used in the core may differ from those declared by the steel manufacturer. For this reason, the characterization of the magnetic properties of the steels directly on the final assembled core already represents an accepted engineering practice [9]–[11]. When it comes to cryogenic machines, little attention has been paid to this aspect, despite its importance in the accurate determination of the core losses, both analytically and using numerical simulations.

This paper investigates the magnetic properties of silicon-iron (SiFe) laminated cores at the ambient and LN_2 temperature. The magnetization characteristics and the core losses are measured under sinusoidal alternating flux density excitation on a fixed stator geometry manufactured using various steel grades. The separation of the total core losses is performed by means of an energy-based engineering approach, which allows to include the influence of the magnetic flux density and the frequency on the loss coefficients. The purpose of this research is a detailed investigation on how the cryogenic temperature influences the magnetic characteristics of the studied cores.

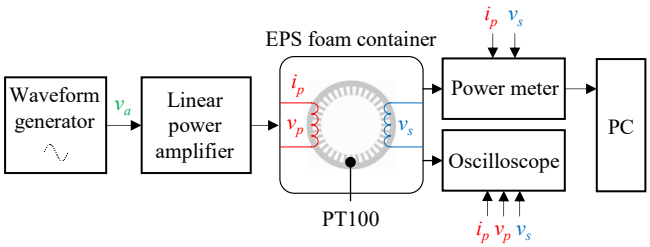

Fig. 1. Schematic of the setup for the magnetic characterization of the cores.

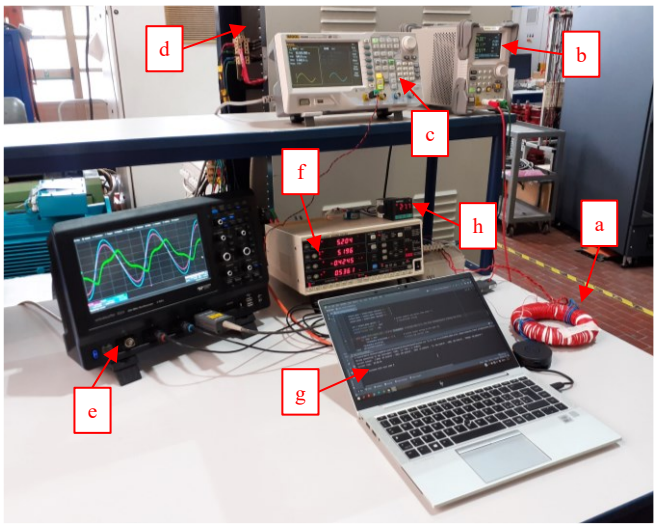

Fig. 2. The setup used for the magnetic characterizations. The core under test at room temperature (a); DC power supply for the temperature sensor (b); waveform generator (c); linear power amplifier (d); oscilloscope (e); high-accuracy digital power meter (f); laptop for the data acquisition (g); the conditioning circuitry for the temperature measurement (h).

II. The Measurement Setup

The characterization of the magnetic properties at room and at the LN_2 temperature was carried out on laminated SiFe stator cores. The laminations have the same geometry, and they were supplied by the same manufacturer with different steel grades: M330-50A, M400-50A and M530-50A. Stress-relief annealing was not applied to the samples after punching. The investigated steel grades are widely adopted in conventional machines for industrial applications, and they are likely to represent a possible choice for cryogenic machines too.

The measurements involved the magnetic characterization of the stator yoke of the samples, which forms a closed magnetic circuit, and is suitable for such engineering investigations [9]. The samples were prepared with a magnetizing (primary) and a sensing (secondary) winding. The former encloses both the yoke and the teeth. The latter instead is placed inside the slots and tightly wrapped in one layer around the stator yoke. The primary winding was realized in two layers to achieve a sufficiently large number of turns for reducing the magnetizing current as much as possible. Furthermore, the cross section of the conductors was chosen large enough to reduce the resistance of the winding. The combination of these two factors allowed to use an open-loop supply scheme for the characterizations, with limited distortion of the electromotive force (emf) induced in the secondary winding, even under moderate saturation of the material.

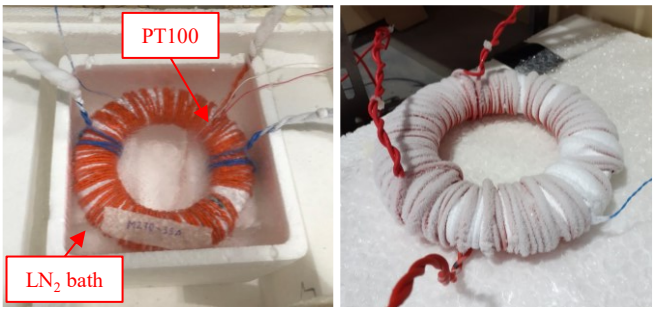

(a) (b)

Fig. 3. The cryogenic testing of the cores. (a) A sample immersed in the liquid nitrogen bath at 77 K; (b) another sample right after the end of the test.

Figure 1 illustrates the schematic of the measurement setup used for the characterizations. The waveform generator imposes a sinusoidal reference voltage v_a (THD < 0.1%) to the linear power amplifier (output bandwidth 5 Hz-40 kHz), which applies the amplified signal v_p to the primary winding of the core under test. A high-accuracy digital power meter was used to measure simultaneously the primary current i_p and the secondary induced emf v_s; the active power associated to the two signals was determined accordingly. Those data were acquired for the post-processing using an in-house acquisition script with a laptop. An oscilloscope recording the primary voltage and current, and the secondary induced emf was used to visualize the distortion of v_s when approaching the magnetic saturation of the steels. An Expanded Polystyrene (EPS) foam container was utilized for the tests at cryogenic temperature. It was filled with LN_2 and the samples were immersed in the cryogenic bath at 77 K. The temperature of the samples was monitored using an RTD PT100 temperature sensor, whose measuring range goes from 73 K to 573 K (–200 °C to 600 °C). The mounted setup during the room temperature tests is shown in Fig. 2.

Figure 3 depicts two of the SiFe cores, one under testing immersed in LN_2 (Fig. 3a) and the other right after the cryogenic tests (Fig. 3b). After the measurements, the samples were dried slowly at ambient temperature. This is necessary to avoid any thermal shock that would likely cause the cracking of the insulation of the windings, which becomes brittle at cryogenic temperature.

The samples were characterized with the described open-loop supply scheme of the measurement setup under sinusoidal alternating flux density excitation. During the measurements the form factor of the secondary induced emf did not deviate from the reference value of 1.11 ± 1% imposed by the standards [12]. Regarding the operating temperature of the samples, a maximum ~15 K increase was detected with regard to the ambient temperature (298 K) during the tests at room temperature, at the highest frequencies. When performing the cryogenic tests, the temperature was always at 77 K.

III. Methodology

The magnetic characterizations included the determination of the magnetization characteristic (*BH* curve), the relative permeability μ_r and the specific core losses of the samples.

The *BH* curves were determined at the supply frequency of 50 Hz, and up to magnetic field intensities H_m ~ 2-2.5 kA/m.

The relative permeability μ_r was calculated accordingly. The specific core losses were determined in two intervals:

- B_m = 0.5-1 T, f = 10-40 Hz;
- B_m = 0.3-1.5 T, f = 50-400 Hz.

B_m is the peak value of the magnetic flux density in the core and f is the excitation frequency. The measurements in the lower frequency range aimed at providing a more precise estimation of the hysteresis losses, as detailed in Section III.C. The measured range of B_m was limited in this case to guarantee the prescribed value for the form factor of v_s. Given the limitations of the used measurement setup, a minimum excitation frequency of 10 Hz was considered low enough to allow a satisfactory engineering estimation of the hysteresis losses. In the higher frequency range, the losses were measured at 50, 75, 100, 150, 200, 300 and 400 Hz.

A. Determination of the magnetization characteristic

The determination of the *BH* curve requires the knowledge of the peak magnetic flux density B_m and the peak magnetic field intensity H_m in the stator yoke. Under sinusoidal flux density excitation, and in the absence of minor hysteresis loops, the values for B_m can be calculated with (1) [13].

$$B_m = \frac{V_{s,rect}}{4 \cdot f \cdot N_s \cdot A} \tag{1}$$

$V_{s,rect}$ is the mean rectified value of the secondary induced emf v_s; f is the excitation frequency; N_s is the number of turns of the secondary winding; A is the cross-sectional area of the stator yoke calculated from its geometrical dimensions. The values for H_m are determined by (2).

$$H_m = \frac{N_p \cdot I_m}{l_{ave}} \tag{2}$$

I_m is the peak value of the primary current i_p; N_p is the number of turns of the primary winding; l_{ave} is the mean length of the magnetic path in the stator yoke. The latter was computed by (3) from the knowledge of the outer D_o and inner D_i diameter of the stator yoke [10].

$$l_{ave} = \frac{\pi \cdot (D_o - D_i)}{\ln(D_o / D_i)} \tag{3}$$

When performing the magnetic characterizations of stator cores, the magnetic flux is not fully guided in the yoke, but locally extends to the tops of the teeth [9]. In this work, such effect was ignored; given the fact that all the tested samples feature the same geometry, the fringing of the magnetic flux lines was reasonably considered to play the same role in all the measurements, for all the materials, at both room and cryogenic temperature.

B. Determination of the specific core losses

The core losses P of the stator yoke can be determined from the active power measured by the power meter, which is obtained from the primary current i_p and the secondary induced emf v_s. The quantity P represents only the power dissipation of the laminated core [13]. The core losses per unit mass p_{Fe} can be obtained dividing P by the mass of the yoke m_a (4).

$$p_{Fe} = \frac{1}{m_a} \cdot \frac{N_p}{N_s} \cdot P = \frac{1}{m_a} \cdot \frac{N_p}{N_s} \cdot \frac{1}{T} \cdot \int_0^T v_s(t) \cdot i_p(t)\, dt \tag{4}$$

p_{Fe} stands for the specific core losses of the stator yoke in W/kg; P is measured by the power meter in W, and T is the electrical period of the supply voltage and current. The factor N_p/N_s is the turn ratio of the primary and secondary windings.

C. Separation of the core losses into components

The separation of the core losses in laminated iron cores can be carried out considering frequency-domain three- or two-term loss models. Both have been used in the analysis of electrical machines.

The three-term loss model segregates the total losses in three contributions: hysteresis, classical and excess losses (5).

$$p_{Fe} = k_h \cdot f \cdot B_m^{\alpha} + k_{cl} \cdot f^2 \cdot B_m^2 + k_{exc} \cdot f^{3/2} \cdot B_m^{3/2} \tag{5}$$

k_h and α are the coefficients of the hysteresis losses, k_{cl} is the coefficient of the classical losses, and k_{exc} is the coefficient of the excess losses.

The two-term loss model splits the total losses in hysteresis and global dynamic components, the latter grouping together classical and excess losses (6).

$$p_{Fe} = k_h \cdot f \cdot B_m^{\alpha} + k_d \cdot f^2 \cdot B_m^2 \tag{6}$$

k_h and α are the coefficients of the hysteresis losses, and k_d is the coefficient of the global dynamic losses. Excess losses can be estimated analytically by considering them as a portion of the global dynamic term [14].

The precise segregation of the total losses into components relies on the correct estimation of the coefficients in (5) and (6). In basic engineering-oriented evaluations, those coefficients are usually calculated by curve-fitting procedures applied to the measured power loss curves. Such approach is inappropriate for two reasons. First, the prediction of the hysteresis losses is physically inconsistent [15]. Second, the coefficients of the dynamic losses in the three-term loss model (5) depend on the physical (k_{cl}, k_{exc}) and microstructural (k_{exc}) properties of the laminations [16], [17]. The global dynamic loss coefficient k_d in (6) depends on the physical properties of the steels only. The values for the coefficients, obtained either from the material properties or by curve fitting, are usually considered as constants, even over wide frequency and flux density ranges. This may lead to inaccurate predictions of the core losses. Focusing the attention on the two-term loss model (6), the values for the loss coefficients can be estimated with an energy-based approach, which better reflects the physical mechanism of the loss phenomena [14], [18]. Furthermore, the accuracy of the loss model can be considerably improved by means of variable loss coefficients [15], [19].

In this research, a two-term loss model was considered. It separates the losses based on an energetic approach and features variable coefficients. The reason behind this choice is mainly because of the geometry of the samples. Indeed, the use of a three-term loss model requires the detailed knowledge of both the physical and microstructural parameters of the steels, that may not be very straightforward to estimate for stator cores.

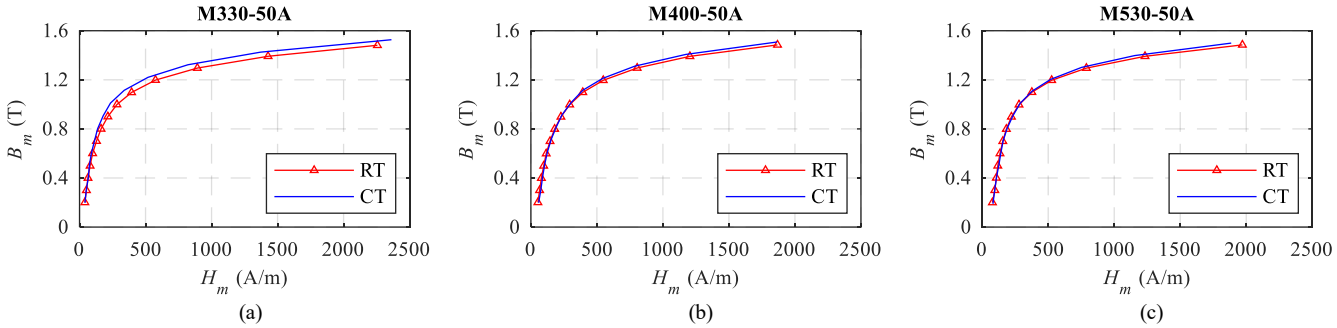

Fig. 4. The *BH* curve of the samples at 50 Hz, room (RT) and cryogenic (CT) temperature. (a) M330-50A, (b) M400-50A, and (c) M530-50A.

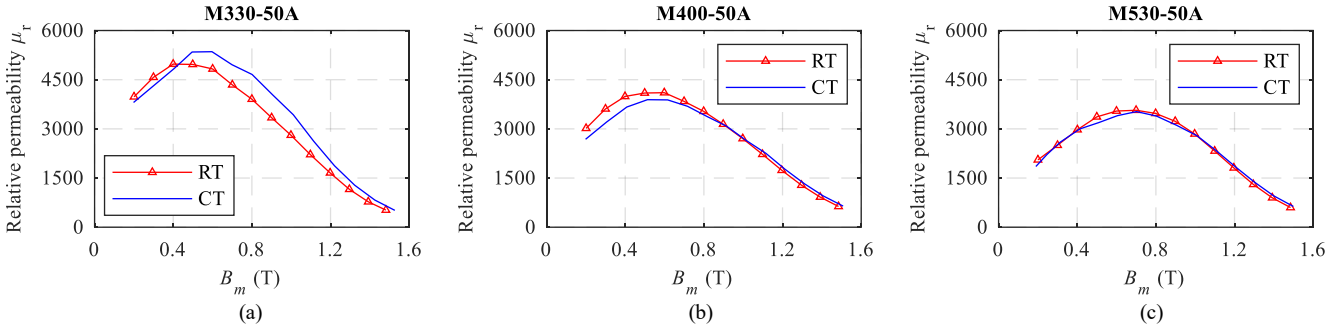

Fig. 5. The relative permeability of the samples at 50 Hz, room (RT) and cryogenic (CT) temperature. (a) M330-50A, (b) M400-50A, and (c) M530-50A.

The considered two-term loss model was proposed in [15], and a slightly different strategy to estimate the hysteresis losses is presented in this research. The specific core losses p_{Fe} are written in (7).

$$p_{Fe}(f,B_m) = k_h(B_m)\cdot f\cdot B_m^2 + k_d(f,B_m)\cdot f^2\cdot B_m^2 \qquad (7)$$

The coefficient α in (6) is assumed equal to 2 in (7). This model considers rate-independent hysteresis losses, which depend only on the magnetic flux density. This assumption holds when the skin effect is negligible, i.e., at sufficiently low frequency [16], [18]. The dependency of the global dynamic losses on both the frequency and the magnetic flux density avoids the use of correction factors for the skin effect [19]. The variable loss coefficients in (7) can be estimated with an energy-based approach. The specific losses per cycle w_{Fe} in J/kg (8) can be obtained dividing (7) by the frequency.

$$w_{Fe}(f,B_m) = k_h(B_m)\cdot B_m^2 + k_d(f,B_m)\cdot f\cdot B_m^2 \qquad (8)$$

When $f\to 0$, the only contribution to the losses per cycle is given by the hysteresis phenomenon, i.e., $w_{Fe|f\to 0} = w_h$ [16]. Such conclusion cannot be drawn from (7), since $p_{Fe|f\to 0} = 0$. Equation (8) allows to estimate the hysteresis losses in accordance with their physical meaning, and k_h can be determined by (9).

$$k_h(B_m) = \frac{w_h}{B_m^2} = \frac{w_{Fe}\big|_{f\to 0}}{B_m^2} \qquad (9)$$

Equation (9) may be employed at sufficiently low frequency, where w_{Fe} follow with good approximation a linear dependence on the frequency, as modeled in (8). This fact was verified in the frequency ranges f = 10-40 Hz and f = 50-100 Hz, and detailed in Section IV. w_h represents the intercept of the energy losses versus frequency curve, linearly extrapolated to zero frequency.

k_d can be calculated for each value of B_m and f by (10).

$$k_d(f,B_m) = \frac{w_{Fe} - w_h}{f\cdot B_m^2} \qquad (10)$$

The contribution of the excess component to the global dynamic losses was not determined in this work.

IV. Results from the Experimental Activities

A. Magnetization characteristic and relative permeability

Figure 4 illustrates the *BH* curves of three steel grades, measured at the magnetizing frequency of 50 Hz, at room (RT) and cryogenic (CT) temperature. The relative permeability μ_r versus B_m is shown in Fig. 5. The magnetization characteristics of the M400 and M530 steel grades show a minor dependence on the temperature over the whole range of H_m. For the M330 grade, a higher dependence was found. Such observations can be drawn especially looking at Fig. 5. The maximum μ_r at CT increases by 7.6% for the M330 grade; for the M400 and M530 grades it decreases by 5.2% and 1.2%, respectively.

It can be concluded that the cryogenic temperature has a marginal influence on the magnetization characteristics of the investigated materials, at 50 Hz and in the analyzed range of B_m.

B. Specific core losses

The specific core losses p_{Fe} of the three steels at 50, 100, 200 and 400 Hz, in the range of B_m = 0.3-1.5 T are reported in Fig. 6. For a better understanding, Tables I-III summarize the results at RT and CT, and at selected values of B_m = 0.5, 1, 1.5 T.

For the M330 steel grade, the increment of the losses at CT is ~7% at 0.5 T, for all the listed frequencies. At 1 T such increment goes from ~5% (50 Hz) to ~10% (400 Hz).

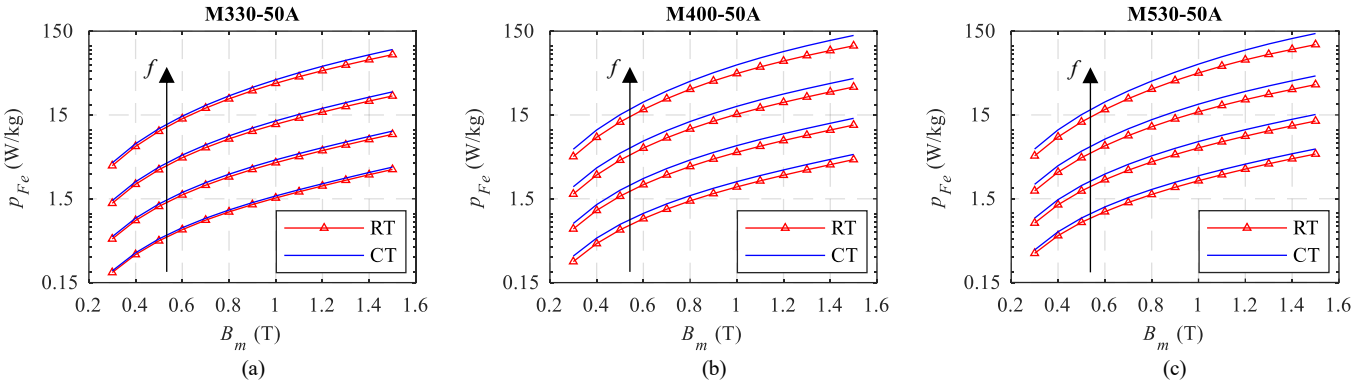

Fig. 6. The specific losses of the samples at f = 50, 100, 200, 400 Hz, room (RT) and cryogenic (CT) temperature. (a) M330-50A, (b) M400-50A, and (c) M530-50A.

TABLE I. SPECIFIC LOSSES OF THE SAMPLES AT DIFFERENT FREQUENCIES: B_m = 0.5 T, ROOM (RT) AND CRYOGENIC (CT) TEMPERATURE

Mat.	p_{Fe} in W/kg at B_m = 0.5 T							
	50 Hz		100 Hz		200 Hz		400 Hz	
	RT	CT	RT	CT	RT	CT	RT	CT
M330	0.47	0.5	1.22	1.3	3.34	3.58	9.6	10.3
M400	0.64	0.74	1.61	1.9	4.34	5.25	12.35	15.1
M530	0.78	0.88	1.86	2.15	4.63	5.54	12.36	15.1

TABLE II. SPECIFIC LOSSES OF THE SAMPLES AT DIFFERENT FREQUENCIES: B_m = 1 T, ROOM (RT) AND CRYOGENIC (CT) TEMPERATURE

Mat.	p_{Fe} in W/kg at B_m = 1 T							
	50 Hz		100 Hz		200 Hz		400 Hz	
	RT	CT	RT	CT	RT	CT	RT	CT
M330	1.54	1.62	4.04	4.37	11.61	12.76	35.78	39.51
M400	2.08	2.4	5.38	6.47	15.3	19	46.81	59.34
M530	2.46	2.82	6.06	7.22	16.34	20.16	47.52	60.62

TABLE III. SPECIFIC LOSSES OF THE SAMPLES AT DIFFERENT FREQUENCIES: B_m = 1.5 T, ROOM (RT) AND CRYOGENIC (CT) TEMPERATURE

Mat.	p_{Fe} in W/kg at B_m = 1.5 T							
	50 Hz		100 Hz		200 Hz		400 Hz	
	RT	CT	RT	CT	RT	CT	RT	CT
M330	3.36	3.58	8.82	9.62	25.3	28.3	78.7	90.55
M400	4.4	5.08	11.37	13.69	32.34	40.83	100.33	133.35
M530	5.13	5.89	12.69	15.19	34.52	43.82	103.64	140.58

The span further increases at 1.5 T, ranging from +6.6% to +15%, at 50 and 400 Hz, respectively.

The M400 and M530 steel grades can be analyzed together. At fixed B_m, they exhibit practically the same behavior over the whole frequency range, at least in terms of relative increase of the losses at CT compared to RT. At 0.5 T, the relative increase of the losses goes from ~16% (50 Hz) to ~22% (400 Hz) for the M400, and from 13% to around 22% for the M530. At 1 T, the increment varies from ~15% to ~27% for both materials. At 1.5 T, it goes from 15% to 33% for the M400, and up to even ~36% for the M530.

C. *Hysteresis and global dynamic loss coefficients*

The separation of the total losses into components requires the knowledge of the k_h and k_d loss coefficients.

Figure 7 depicts the losses per cycle versus frequency of the M400 steel at RT and CT; the markers indicate the measurement frequencies. For brevity, such curves are reported for the M400 steel grade only. The linear fit in Fig. 7a and Fig. 7b is in good agreement with the measurements ($R^2 \geq 0.98$). This means that (8) models accurately the energy losses w_{Fe} in the examined frequency and flux density ranges. The measurements in the interval 10-40 Hz, 0.5-1 T (Fig. 7a), were performed to provide reference values for w_h at RT and CT. For the separation of the losses in the frequency range 50-400 Hz, B_m = 0.3-1.5 T, w_h was estimated extrapolating to f = 0 the losses per cycle in the interval 50-100 Hz as in Fig. 7b. At 1 T, RT, the estimation of w_h extrapolating the energy losses from the range 50-100 Hz is 7%, 4.7% and 2.5% higher than the reference values obtained from the range 10-40 Hz, for the M330, M400 and M530 steels, respectively. Such increase becomes 9%, 4.7% and 3.3% at CT. For all the steels, the maximum difference remains within a maximum of +15% at 0.5 T. The comparison shows that w_h determined from the measurements at 50-100 Hz is slightly overestimated, especially at B_m < 1 T. However, the majority of the core in electrical machines usually operates above 1 T, and special equipment is necessary for the loss measurements at low frequency and in a wide range of flux density. For this reason, w_h estimated from the measurements in the range 50-100 Hz was considered suitable for the engineering investigations presented in this research. Also, this does not affect the accuracy of (7) in predicting the total losses.

Figure 8 shows the coefficient $k_h(B_m)$ computed from the measurements at RT and CT in the interval 50-100 Hz, B_m = 0.3-1.5 T. In the range B_m = 1-1.5 T, the average relative increase of k_h at CT for the M330, M400 and M530 steels is 1.5%, 6.7% and 7.1%, respectively. Such results show a marginal increase of the hysteresis losses at CT, especially for the M330 steel grade.

Figures 9-11 show the computed global dynamic loss coefficient $k_d(f, B_m)$ for all the three materials, at RT and CT. Looking at the results for the M330 steel at 1 T in Fig. 9, the value for k_d decreases with the frequency, especially at 200 and 400 Hz, at both RT and CT. This fact demonstrates that in (8), at fixed B_m, the slope of the energy losses versus frequency curves (k_d) should not be considered constant.

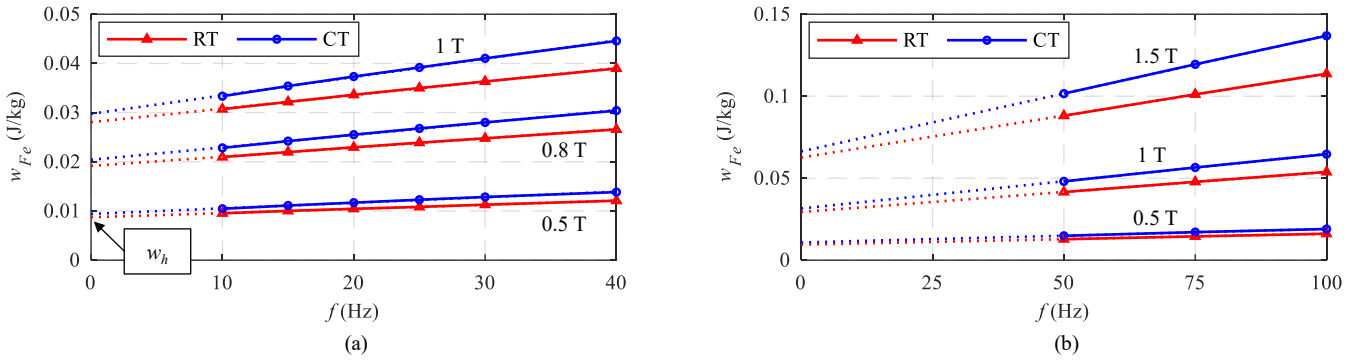

Fig. 7. The estimation of the specific hysteresis losses per cycle w_h for the M400-50A sample at room (RT) and cryogenic (CT) temperature. (a) Energy losses in the frequency range 10-40 Hz; (b) energy losses in the frequency range 50-100 Hz. The dotted lines represent the linear extrapolation to zero frequency.

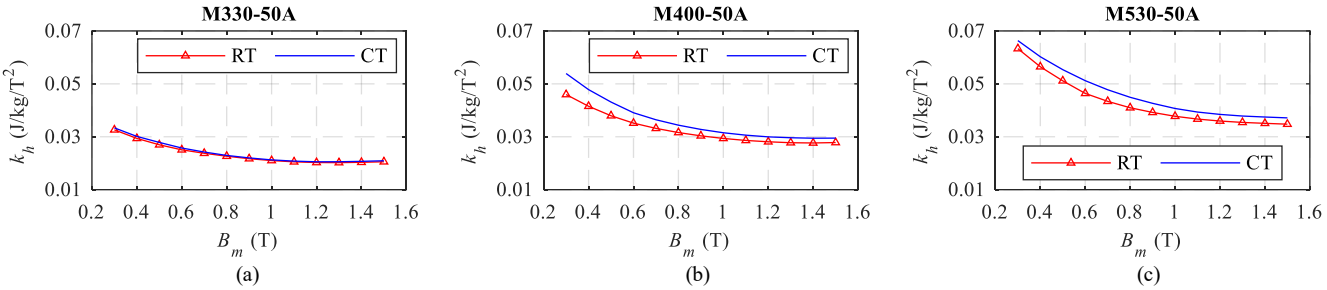

Fig. 8. The variable hysteresis loss coefficient $k_h(B_m)$ at room (RT) and cryogenic (CT) temperature computed from the estimation of w_h in the frequency range 50-100 Hz and in the flux density range 0.3-1.5 T. (a) M330-50A, (b) M400-50A, and (c) M530-50A.

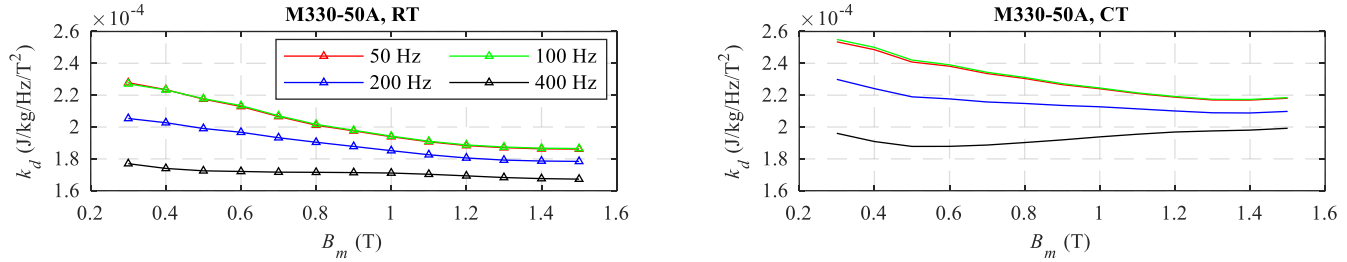

Fig. 9. The variable global dynamic loss coefficient $k_d(f, B_m)$: M330-50A sample, f = 50-400 Hz, B_m = 0.3-1.5 T. (a) Room (RT), and (b) cryogenic (CT) temperature.

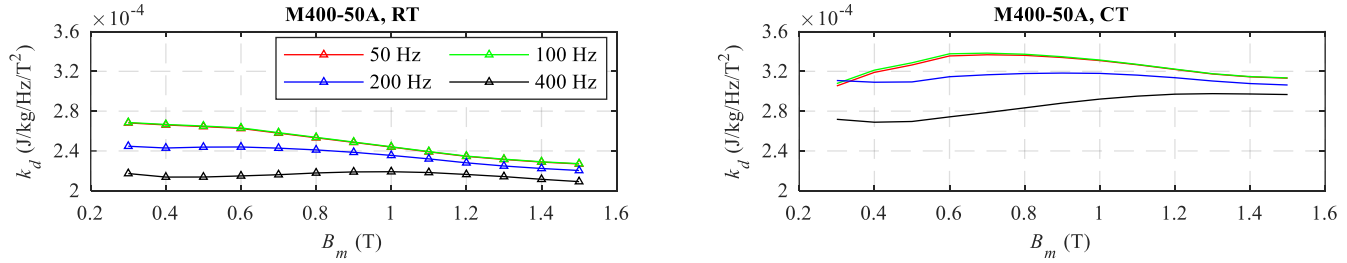

Fig. 10. The variable global dynamic loss coefficient $k_d(f, B_m)$: M400-50A sample, f = 50-400 Hz, B_m = 0.3-1.5 T. (a) Room (RT), and (b) cryogenic (CT) temperature.

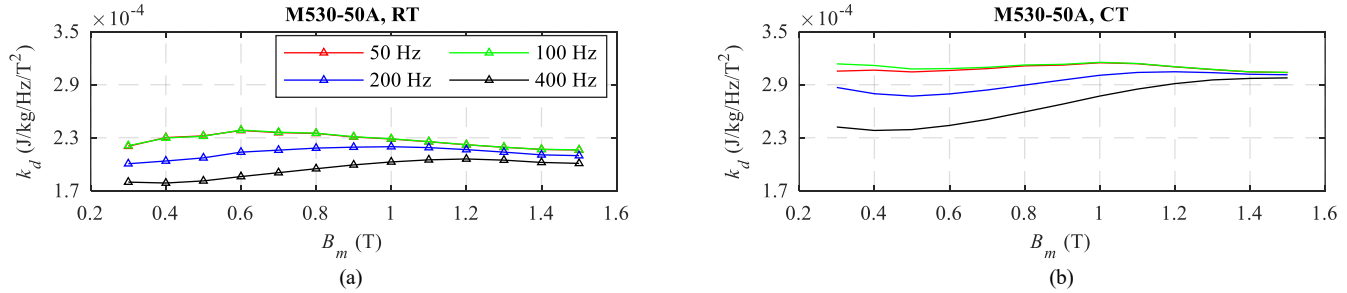

Fig. 11. The variable global dynamic loss coefficient $k_d(f, B_m)$: M530-50A sample, f = 50-400 Hz, B_m = 0.3-1.5 T. (a) Room (RT), and (b) cryogenic (CT) temperature.

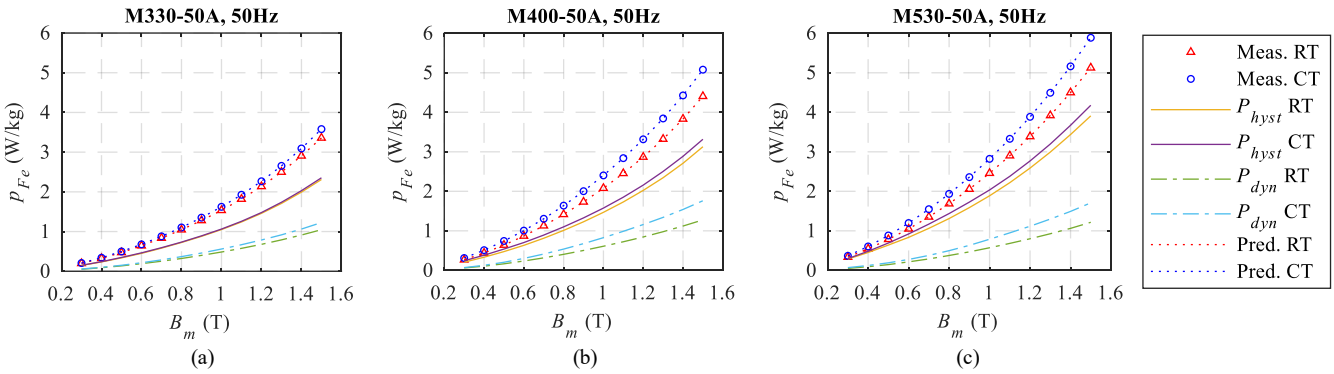

Fig. 12. The separation of the specific losses at room (RT) and cryogenic (CT) temperature, f = 50 Hz. (a) M330-50A, (b) M400-50A, and (c) M530-50A.

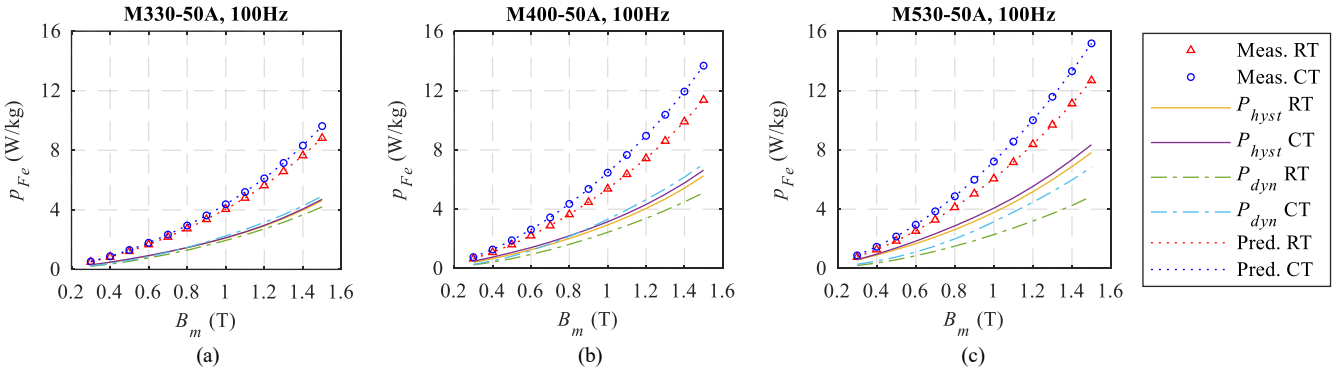

Fig. 13. The separation of the specific losses at room (RT) and cryogenic (CT) temperature, f = 100 Hz. (a) M330-50A, (b) M400-50A, and (c) M530-50A.

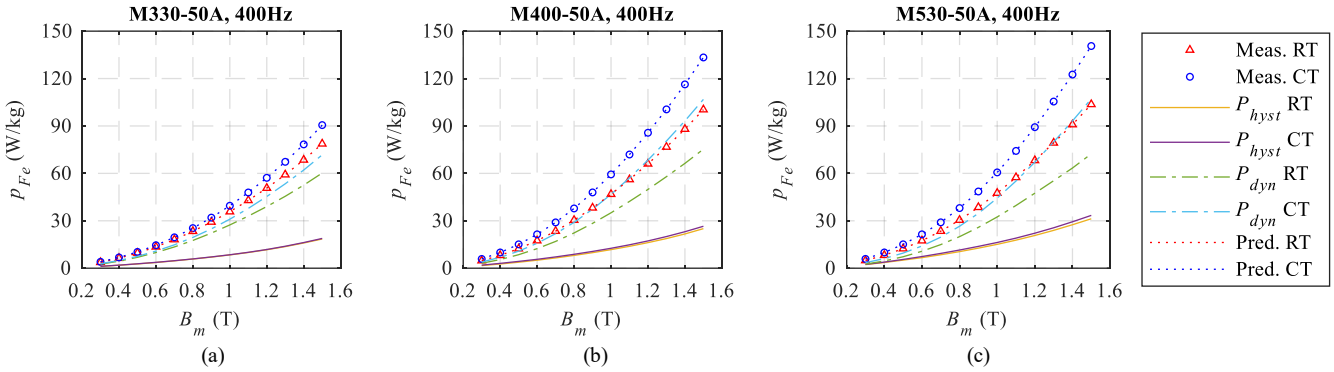

Fig. 14. The separation of the specific losses at room (RT) and cryogenic (CT) temperature, f = 400 Hz. (a) M330-50A, (b) M400-50A, and (c) M530-50A.

A similar behavior can be observed for the M400 and M530 steels as well, see Figs. 10-11. For all the materials it is curious to see that the k_d versus B_m curves at 50 and 100 Hz are very similar. In addition, at different frequencies, such curves tend to approach each other above 1.2 T; this is especially true for the M530 steel grade, as visible in Fig. 11.

The influence of the cryogenic temperature on k_d is well evident for all the steels, and it can be physically explained, at least in part, by the reduction of their resistivity at CT. This causes an increase of the eddy current related phenomena, thus leading to an increase of the global dynamic losses. Comparison of the values for k_d at RT and CT, and B_m = 1 T, shows a similar relative increase at all the investigated frequencies. On average, k_d augments at CT by 15%, 35% and 37.5% for the M330, M400 and M530 steels, respectively. At 1.5 T those percentage increases become 18%, 39% and 43.5%. This directly reflects on the significant increase of the global dynamic losses at CT.

D. Separation of the losses at selected frequencies

Figures 12-14 show the results of the loss separation carried out for all the three tested samples; due to the space limitations, the loss separation is only discussed at 50, 100 and 400 Hz.

The use of the two-term loss model (7) allowed to obtain very accurate results of the loss prediction over a wide range of frequency and magnetic flux density. As seen from Figs. 12-14, the predicted losses (Pred) are in exact agreement with the measured ones (Meas). This is because of using the variable loss coefficients. At 50 Hz, the hysteresis losses (P_{hyst}) are predominant for all the three steels, while the global dynamic losses (P_{dyn}) represent the major contribution at 400 Hz.

The contribution of the loss components at CT and RT is well visible when plotting the specific losses versus flux density curves, Figs. 12-14. This highlights better the results obtained for the coefficients k_h and k_d presented in Section IV.C.

V. Discussion

After presenting all the results, few comments about the examined core loss model are still necessary.

The use of a frequency-domain model is suitable for the investigations on the losses presented in this paper. Indeed, the samples were tested under sinusoidal flux density excitation and at single magnetizing frequencies, i.e., no higher harmonics are considered to appear in its harmonic spectrum.

The use of an energy-based approach for the calculation of the loss coefficients allows to obtain a realistic separation of the total losses into the hysteresis and global dynamic components. The use of variable loss coefficients is not the result of a purely numerical manipulation of the measurement data, but it comes from their physical-based post-processing. The separation of the excess losses from the global dynamic term can be challenging, especially when using variable loss coefficients [19]. However, the method described in [14] could be adapted to (7) too, provided that the electrical conductivity of the steels is known.

It was verified that the model (8) describes well the energy losses in the steels analyzed in this paper even in the extended frequency range 50-400 Hz, with an R^2 value always > 0.98.

VI. Conclusion

The present paper investigated the magnetic properties of different silicon-iron (SiFe) laminated cores at room and at the LN_2 temperature. Three cores with the same geometry and manufactured using M330-50A, M400-50A and M530-50A steel grades were characterized in terms of both their magnetization characteristic and specific core losses.

The magnetization characteristic was measured at 50 Hz, and the results showed that the cryogenic temperature has a marginal effect on it. The core losses were measured under sinusoidal alternating flux density excitation, and the separation into physical components was carried out by means of a two-term loss model with variable coefficients. The results revealed that the core losses at cryogenic temperature are generally higher than those at room temperature. The M400 and M530 steels exhibited a substantial increase of the core losses at cryogenic temperature, while the M330 grade was less influenced.

The energy-based separation of the core losses into the hysteresis and the global dynamic loss components provided reasonable results. It also revealed that in general the cryogenic temperature does influence the global dynamic losses, while the hysteresis losses are not much affected.

The presented model can be used in numerical simulations for computing the core losses in electrical machines. The good accuracy of the model for conventional electrical machines has been already discussed in the literature. Future works will focus on its applicability to cryogenic electrical machines, where the accurate estimation of the core losses is of capital importance.

Acknowledgment

This work has been supported by the COMET-K2 "Center for Symbiotic Mechatronics" of the Linz Center of Mechatronics (LCM) funded by the Austrian federal government and the federal state of Upper Austria.

References

[1] M. Biasion, J. F. P. Fernandes, S. Vaschetto, A. Cavagnino, and A. Tenconi, "Superconductivity and its Application in the Field of Electrical Machines," in 2021 IEEE International Electric Machines & Drives Conference (IEMDC), May 2021, pp. 1–7.

[2] M. Biasion, F. P. Joao Fernandes, P. J. da C. Branco, S. Vaschetto, A. Cavagnino, and A. Tenconi, "A Comparison of Cryogenic-Cooled and Superconducting Electrical Machines," in 2021 IEEE Energy Conversion Congress and Exposition (ECCE), Oct. 2021, pp. 4045–4052.

[3] J. J. Gniewek and E. Ploge, "Cryogenic behavior of selected magnetic materials," *J. Res. NBS-Eng. Instrum.*, vol. 69C, no. 3, pp. 225–236, 1965.

[4] X. Pei, A. C. Smith, L. Vandenbossche, and J. Rens, "Magnetic Characterization of Soft Magnetic Cores at Cryogenic Temperatures," *IEEE Trans. Appl. Supercond.*, vol. 29, no. 5, pp. 1–6, Aug. 2019.

[5] P. Breining, M. Veigel, M. Doppelbauer, Y. Liu, and M. Noe, "Iron loss measurement of nonoriented silicon and cobalt iron electrical steel sheets at liquid nitrogen temperature using ring specimen," in 2017 IEEE International Electric Machines and Drives Conference (IEMDC), May 2017, pp. 1–7.

[6] Y. Liu, M. Noe, J. Ou, P. Breining, M. Veigel, and M. Doppelbauer, "Measurement of Magnetic Materials at Room and Cryogenic Temperature for Their Application to Superconducting Wind Generators," *IEEE Trans. Appl. Supercond.*, vol. 28, no. 3, pp. 1–6, Apr. 2018.

[7] D. Miyagi, D. Otome, M. Nakano, and N. Takahashi, "Measurement of Magnetic Properties of Nonoriented Electrical Steel Sheet at Liquid Nitrogen Temperature Using Single Sheet Tester," *IEEE Trans. Magn.*, vol. 46, no. 2, pp. 314–317, Feb. 2010.

[8] M. Miyamoto, T. Matsuo, and T. Nakamura, "Measurement of vector hysteretic property of silicon steel sheets at liquid nitrogen temperature," *Przegląd Elektrotechniczny*, vol. 87, no. 9b, p. 4, 2011.

[9] A. J. Clerc and A. Muetze, "Measurement of Stator Core Magnetic Degradation During the Manufacturing Process," *IEEE Trans. Ind. Appl.*, vol. 48, no. 4, pp. 1344–1352, Jul. 2012.

[10] A. Krings and J. Soulard, "Experimental characterization of magnetic materials for electrical machine applications," in 2015 IEEE Workshop on Electrical Machines Design, Control and Diagnosis (WEMDCD), Mar. 2015, pp. 85–89.

[11] L. Masisi, M. Ibrahim, J. Wanjiku, A. M. Aljehaimi, and P. Pillay, "The Effect of Two- and Three-Level Inverters on the Core Loss of a Synchronous Reluctance Machine (SynRM)," *IEEE Trans. Ind. Appl.*, vol. 52, no. 5, pp. 3805–3813, Sep. 2016.

[12] "Standard Test Method for Alternating-Current Magnetic Properties of Toroidal Core Specimens Using the Voltmeter-Ammeter-Wattmeter Method," ASTM Stand. A927/A927M-18, 2018.

[13] F. Fiorillo, *Characterization and Measurement of Magnetic Materials*. Elsevier Academic Press, 2004.

[14] K. Yamazaki, A. Suzuki, M. Ohto, and T. Takakura, "Harmonic Loss and Torque Analysis of High-Speed Induction Motors," *IEEE Trans. Ind. Appl.*, vol. 48, no. 3, pp. 933–941, May 2012.

[15] E. Dlala, M. Solveson, S. Stanton, and A. Arkkio, "Improved Model for the Prediction of Core Loss in Finite Element Analysis of Electric Machines," in 2015 IEEE International Electric Machines & Drives Conference (IEMDC), May 2015, pp. 340–344.

[16] G. Bertotti, "General properties of power losses in soft ferromagnetic materials," *IEEE Trans. Magn.*, vol. 24, no. 1, pp. 621–630, 1988.

[17] D. Kowal, P. Sergeant, L. Dupre, and L. Vandenbossche, "Comparison of Iron Loss Models for Electrical Machines With Different Frequency Domain and Time Domain Methods for Excess Loss Prediction," *IEEE Trans. Magn.*, vol. 51, no. 1, pp. 1–10, Jan. 2015.

[18] M. Ibrahim and P. Pillay, "Advanced Testing and Modeling of Magnetic Materials Including a New Method of Core Loss Separation for Electrical Machines," *IEEE Trans. Ind. Appl.*, vol. 48, no. 5, pp. 1507–1515, Sep. 2012.

[19] D. M. Ionel, M. Popescu, M. I. McGilp, T. J. E. Miller, S. J. Dellinger, and R. J. Heideman, "Computation of Core Losses in Electrical Machines Using Improved Models for Laminated Steel," *IEEE Trans. Ind. Appl.*, vol. 43, no. 6, pp. 1554–1564, 2007.